# Green-Assisted Synthesis and Multi-Functional Evaluation of TiO<sub>2</sub>–ZrO<sub>2</sub>–Cu Nanocomposite for Enhanced Antibacterial, Antioxidant, and Anticancer Performance

<sup>1</sup>S. Ayyappan,

Assistant Professor, Department of Physics,
Government College of Technology, Coimbatore, India

sayyappanraj@gmail.com

<sup>2</sup>S. Murugan

Assistant Professor, \* Department of Civil Engineering, Government College of Technology, Coimbatore, India

smurugan02@gmail.com

**Corresponding author:** 

3,\*M. Rama

Assistant Professor, Department of Civil Engineering, Government College of Technology, Coimbatore, India

ramamahal@gmail.com

# **Abstract**

This study presents a novel eco-friendly synthesis approach for multi-metallic  $TiO_2$ – $ZrO_2$ –Cu nanocomposites using a facile hydrothermal-assisted and chemical reduction method. Zirconia ( $ZrO_2$ ) and titania ( $TiO_2$ ) nanoparticles were synthesized and doped in two compositions (30% and 15%  $ZrO_2$  in  $TiO_2$ ), followed by integration with copper nanoparticles (CuNPs). The structural, morphological, and optical properties were analyzed using XRD, FTIR, UV-Vis, SEM, and HRTEM techniques. The synthesized materials exhibited high crystallinity and uniform dispersion with particle sizes below 50 nm. Antibacterial evaluation via the disc diffusion assay confirmed significant inhibition zones against both Gram-positive and Gram-negative pathogens, surpassing pure oxides. The nanocomposite also demonstrated superior antioxidant activity through DPPH, FRAP,  $H_2O_2$ , hydroxyl radical, and nitric oxide scavenging assays. Furthermore, in vitro MTT assays on MCF-7 breast cancer cell lines revealed dose-dependent cytotoxicity, with induced apoptosis confirmed via Bcl-2 gene suppression and elevated caspase-3 and -9 activities. The catalyst also achieved remarkable dye degradation efficiency against methylene blue and Congo red. The study establishes  $TiO_2$ – $ZrO_2$ –Cu nanocomposites as multifunctional materials for biomedical and environmental remediation applications.

**Keywords:** TiO<sub>2</sub>–ZrO<sub>2</sub>–Cu nanocomposite, Green synthesis, Antibacterial activity, Antioxidant performance, Anticancer properties and Photocatalytic degradation.

### 1. Introduction

Nanotechnology has emerged as one of the most transformative areas in modern materials science, enabling the design of multifunctional nanomaterials with tailored structural, optical, and biological properties. Among various nanomaterials, transition metal oxides such as titanium dioxide (TiO<sub>2</sub>) and zirconium dioxide (ZrO<sub>2</sub>) have attracted significant attention due to their excellent chemical stability, photocatalytic efficiency, and biocompatibility. TiO<sub>2</sub>, a well-known semiconductor oxide, exhibits outstanding photocatalytic and antibacterial activity; however, its practical applications are often limited by

ISSN: 1750-9548

a wide band gap (3.2 eV) and high electron-hole recombination rate. To overcome these challenges, the incorporation of dopants and the formation of mixed-oxide nanocomposites have been proven effective strategies for enhancing charge separation and broadening light absorption.

ZrO<sub>2</sub>, with its high thermal stability, mechanical robustness, and low toxicity, is an ideal candidate to form binary or ternary composites with TiO<sub>2</sub>, improving both structural stability and electronic characteristics. The introduction of copper (Cu) nanoparticles further enhances the system's redox potential, surface plasmon resonance, and catalytic activity, making the TiO<sub>2</sub>–ZrO<sub>2</sub>–Cu hybrid a promising platform for a wide range of biomedical and environmental applications. Cu nanoparticles are known for their potent antibacterial and anticancer properties due to their ability to generate reactive oxygen species (ROS) and induce oxidative stress in microbial and cancer cells.

In recent years, green synthesis methods have gained considerable importance as sustainable alternatives to conventional chemical routes. Traditional synthesis processes often involve toxic reagents, high temperatures, and hazardous byproducts, which pose environmental and health risks. In contrast, green-assisted synthesis utilizes eco-friendly precursors, plant extracts, or mild reducing agents, ensuring minimal environmental impact while preserving nanoparticle stability and biocompatibility. The development of such environmentally benign techniques aligns with the principles of green chemistry and sustainable nanotechnology.

The integration of TiO<sub>2</sub>, ZrO<sub>2</sub>, and Cu through a green-assisted hydrothermal and chemical reduction method is expected to yield a nanocomposite with synergistic multifunctionality. The combined properties of enhanced photocatalytic degradation, strong antibacterial action, efficient radical scavenging, and selective cytotoxicity toward cancer cells make this system highly attractive for biomedical therapeutics and environmental remediation. Despite several studies on binary TiO<sub>2</sub>–Cu and TiO<sub>2</sub>–ZrO<sub>2</sub> systems, limited research has focused on the synergistic effects of ternary TiO<sub>2</sub>–ZrO<sub>2</sub>–Cu nanocomposites synthesized via eco-friendly routes. Therefore, the present study aims to synthesize TiO<sub>2</sub>–ZrO<sub>2</sub>–Cu nanocomposites using a green-assisted hydrothermal and chemical reduction approach and to comprehensively evaluate their structural, optical, and multifunctional biological performance. The materials were characterized using XRD, FTIR, UV-Vis, SEM, and HRTEM techniques, and their antibacterial, antioxidant, and anticancer activities were systematically analyzed. The findings highlight the potential of this ternary nanocomposite as an efficient, sustainable, and multifunctional material for next-generation biomedical and environmental applications.

# 2. Experimental Methods

# 2.1. Equipments

UV-Vis spectrophotometer (Varian, Carry 5000) spectrophotometer was used to measure absorption with 1-cm path length quartz cuvettes, FTIR spectrophotometer (Thermo Nicolet, Avatar 370) was employed for embedded function group identification and Bruker AXS Advance powder X-ray diffractometer was used for characterisation of crystalline nature of sample. Morphological analyses were carried out using Scanning Electron Microscopy (SEM) with a JEOL Model JSM - 6390LV instrument and Jeol/JEM 2100 High Resolution Transmission Electron Microscope.

### 2.2. Chemicals and Microbial Cultures

Zirconium nitrate pentahydrate Zr(NO<sub>3</sub>)<sub>4-5H2O</sub>, Titanium nitrate tetra hydrate Ti(NO<sub>2</sub>)<sub>4</sub>.4H<sub>2</sub> O, and urea were purchased from HiMedia. Copper acetate (Cu(CH<sub>3</sub> COO)<sub>2</sub>), sodium hydroxide (NaOH), ethanol (CH<sub>3</sub> CH<sub>2</sub> OH) and L-ascorbic acid (C<sub>6</sub> H<sub>8</sub> O<sub>6</sub>) were purchased from Sigma–Aldrich, Germany and used without further purification. All the experiments and preparations have been performed using milli-Q water (Millipore, Milford, MA, USA). All glassware were washed with sterile distilled water and then rinsed with deionized water.

All the chemicals used in this work were of analytical grades. Milli-Q distilled water was used for nanoparticle synthesis. Gram positive bacteria (Bacillus subtilis MTCC 1305 and Staphylococcus aureus MTCC 3160) and gram negative bacteria (Escherichia coli MTCC 443 and Pseudomonas aeruginosa MTCC 2453) were procured from Microbial Type Culture Collection (MTCC) and used as test organisms. All the cultures were stored and maintained at 4<sup>o</sup> C.

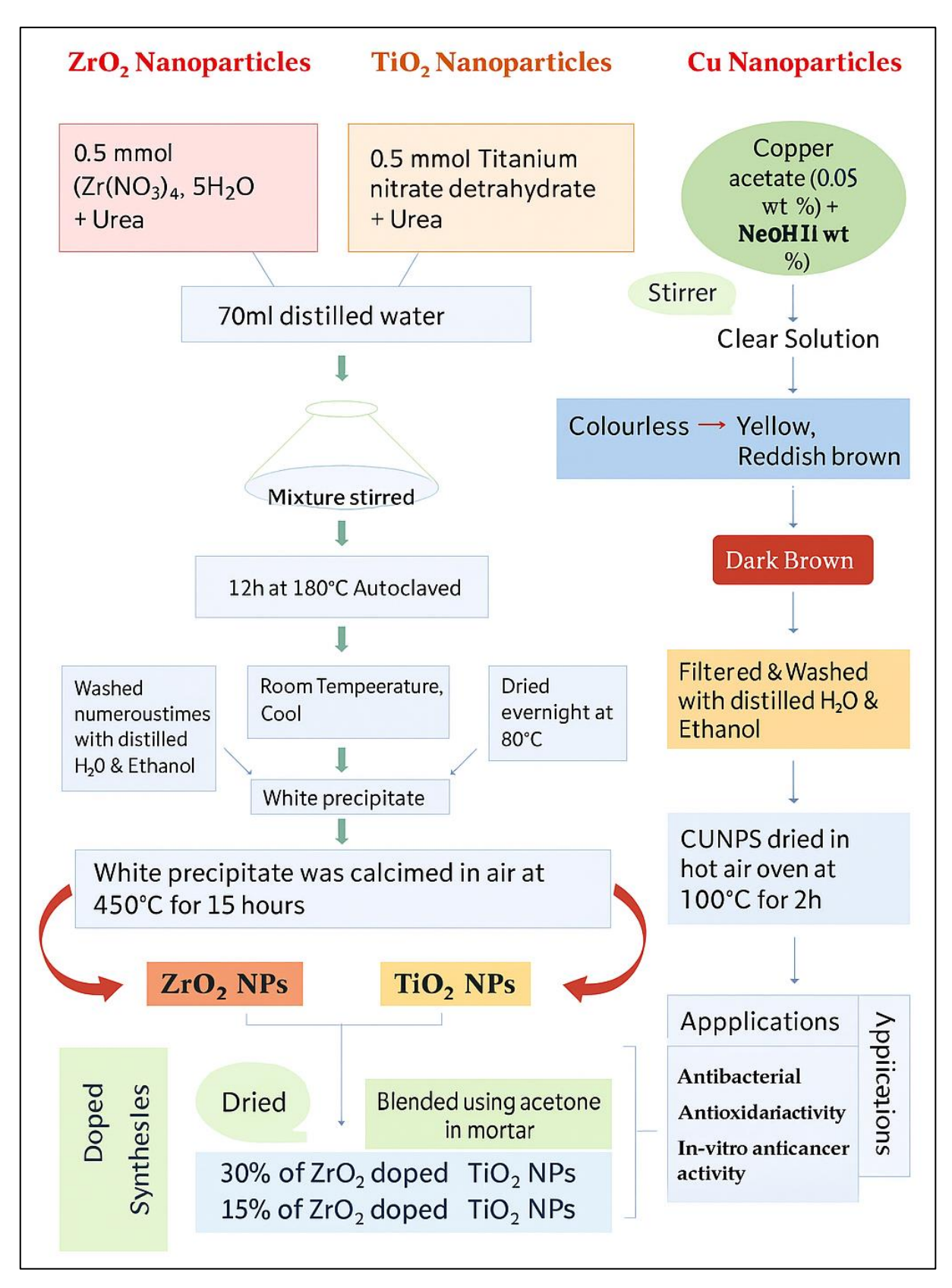


Figure 1: Synthesis of Nanoparticles and their Applications

### 2.3. Synthesis of Metal and Metal Oxide Nanoparticles

# 2.3.1. Synthesis of ZrO<sub>2</sub> Nanoparticles

Synthesis of ZrO<sub>2</sub> NPs was carried out as follows: 0.5 mmol of Zr(NO<sub>3</sub>)<sub>4</sub>.5H<sub>2</sub> O and a trivial quantity of urea (CO(NH2)2) were dissolved in 70 ml of deionized water and the mixture was continuously stirred. Then, the homogenous solution was transferred into a 100 ml conical flask, teflon lined and autoclaved for 12 h at 180 C. Once the process was completed, the solution was shifted to room temperature and allowed to cool. Finally, a white precipitate was formed. The precipitate was washed numerous times with plenty of distilled water and absolute ethanol and subsequently dried overnight at 80° C. Eventually, the white precipitate was claimed in air at 450° C for 15 h.

### 2.3.2. Synthesis of TiO<sub>2</sub> Nanoparticles

Synthesis of TiO<sub>2</sub> NPs was carried out as follows: 0.5 mmol of Titanium nitrate tetrahydrate Ti(NO<sub>3</sub>)<sub>4</sub>.4H<sub>2</sub> O and a trivial quantity of urea (CO(NH<sub>2</sub>)<sub>2</sub>) were dissolved in 70 ml of deionized water and the mixture was continuously stirred. Then, the homogenous solution was transferred into a 100ml conical flask, teflon lined and autoclaved for 12 h at 180 °C. Once the process was completed, the solution was then shifted to room temperature and allowed to cool. Finally, a white precipitate was

formed. The precipitate was washed numerous times with plenty of distilled water and absolute ethanol and subsequently dried overnight at 80° C. Eventually, the white precipitate was dried in air at 450° C for 15hours.

### 2.3.3. Synthesis of ZrO<sub>2</sub> Nanoparticles doped with TiO<sub>2</sub> Nanoparticles

The synthesized above oxides were mixed in two different compositions, 70% of TiO<sub>2</sub> with 30% of ZrO<sub>2</sub> and 85% of TiO<sub>2</sub> with 15% of ZrO<sub>2</sub>. Each composition was blended using acetone in mortar, dried and labelled as 30% ZrO<sub>2</sub> doped TiO<sub>2</sub> NPs and 15% ZrO<sub>2</sub> dopedTiO2NPs.

### 2.3.4. Synthesis of Cu Nanoparticles

The synthesis of CuNPs was carried out using the modification of a typical chemical reduction procedure. Copper acetate (0.05 wt %) was mixed with sodium hydroxide (1 wt %) and subjected to constant stirring using a magnetic stirrer to attain a clear solution. The reducing agent, L-ascorbic acid (2.5 wt %) was added drop-wise to the mixture. With the increase in time, the colour of the solution gradually turned from colourless to yellow, reddish brown and finally to dark brown. The occurrence of yellow colour denoted the initiation of the reduction reaction [46]. Reduction was permitted to continue for 15 min so as to ensure complete reduction of copper acetate. The precipitated CuNPs were filtered, washed with distilled water and later using ethanol. CuNPs were finally dried in a hot air oven at 100 °C for 2 h. Optimization studies were then conducted to explore the size and shape of CuNPs [11].

# 2.4. Characterisation of Metal and Metal Oxide Nanoparticles

# 2.4.1. Characterisation of ZrO<sub>2</sub> Nanoparticles

The morphology and the size of the ZrO<sub>2</sub> NPs were characterized by Scanning Electron Microscopy (SEM). ZrO<sub>2</sub> NPs size, morphology and distribution were examined by the High-Resolution Transmission Electron Microscope. UV-V is spectrophotometer was used to measure the absorption spectra of the synthesized nanoparticles in the range of 175-3300 nm. The readings were taken at intervals of 1 nm with the scan rate 600 nm/min. The as-prepared nanoparticles were subjected to functional group analysis using FTIR spectrophotometer. The samples were prepared using KBr pellet method in 1:99 ratios at room temperature. The samples were scanned in the spectral range of 4000-400 cm-1 with the resolution of 2 cm-1 . X-ray diffraction (XRD) patterns were collected using a powder X-ray diffractometer. The XRD pattern of synthesized sample was obtained inside the special XRD cell designed to avoid the reaction of air sensitive samples with atmospheric oxygen [12].

# 2.4.2. Characterisation of TiO2 Nanoparticles

TiO<sub>2</sub>Nps were characterized using the same method of ZrO<sub>2</sub>Nps.

# 2.4.3. Characterisation of the Synthesized TiO<sub>2</sub> doped ZrO<sub>2</sub> Nanoparticles

The absorption spectra of 70 and 85% TiO<sub>2</sub> doped ZrO<sub>2</sub>NPs were evaluated inthe range of 175-3300 nm at the interval of 1 nm with the scanning rate of 600nm/min using Varian, Carry 5000 model UV –Vis Spectrophotometer. Both the TiO<sub>2</sub> doped ZrO<sub>2</sub>NPswere subjected to functional group analysis using Thermo Nicolet, Avatar 370 model Fourier Transmittance Infra-Red (FTIR) spectrophotometer. The surface morphology and distribution of zirconia and titanium dioxide were examined through JEOL Model JSM - 6390LV Scanning Electron Microscopy (SEM) and Jeol/JEM 2100 High Resolution Transmission Electron microscope (TEM). Bruker AXS Advance powder X-ray diffractometer was used for crystalline characterisation of the synthesized nanoparticles and specially designed XRD cell was used to avoid the reaction of the sample with air [1].

### 2.4.4. Characterisation of Cu Nanoparticles

The absorption spectra of the synthesized CuNPs were recorded as a function of time using a Shimadzu, UV-2600, UV-visible spectrometer. FT-IR spectra were recorded on a Perkin-Elmer 100 series with KBr as the reference material to studytheinteractions between the zero valent copper nanoparticles and the reducing agent, Lascorbic acid. Morphology of the CuNPs was investigated by a Hitachi Field Emission Scanning Electron Microscope. X-Ray Diffraction measurements were performed using a PANalytical, X'Pert, X-ray diffractometer using Cu K $\alpha$  radiation ( $\lambda$ = 1.54056A $^{\circ}$ ) so as to confirm the phase confirmation and crystalline nature of CuNPs. To confirm the size and homogenous shape of the CuNPs, transmission electron micrographs were acquired using a JEM-1011; JEOL microscope working at an accelerating voltage of 200 kV. Samples for transmission electron microscopy (TEM) were made ready by direct deposition on a carbon-coated copper grid. Size of the CuNPs was determined by DLS in back scattering mode, using Malvern 110 Zetasizer at 25 °C[12]

### 2.5. Antibacterial activity of metal oxide Nanoparticles

### 2.5.1. Antibacterial assay of ZrO2 nanoparticles

The antimicrobial activity of the ZrO<sub>2</sub>NPs was evaluated with well disc diffusion method [2]. The experiment was conducted against reference gram positive (Bacillussubtilis and Staphylococcusaureus) and gram negative bacteria (E.coliand P. aeruginosa) procured from Microbial Type Culture Collection (MTCC), Chandigarh, India. An inoculum size of 105 cells/ml was used to spread on the Mueller-Hinton Agar (MHA, HiMedia, India). In Brief, 20 ml of MHA was poured into petri dishes and allowed to solidify. Then, 6 mm thick sterile discs were placed appropriately on petridishes. Finally, different concentrations of ZrO<sub>2</sub>Nps (20, 40, 80 and 100 mg/ml) were loaded on each disc and 50% ethanol was used as a negative control. All the plates were incubated at 370 C for 24 h and the respective inhibition zones were measured. Each test was performed in triplicates under the same set of conditions for reproducibility [3].

### 2.5.2. Antibacterial Assay of TiO2 Nanoparticles

Antibacterial activity of TiO2Nps was evaluated using the above well disc diffusion method.

# 2.5.3. Antibacterial Assay of the Synthesized TiO2 doped ZrO2 Nanoparticles

The disc diffusion method [2] was employed to identify the antimicrobial activities of the synthesized nanoparticles against the reference gram positive and negative bacteria. Mueller- Hinton Agar ((MHA, Himedia, India) was used to spread the inoculum size of 105 cells/ml. Initially, 20 ml of agar solution was poured into petridishes and allowed to solidify, then, 6 mm thick sterile discs were placed appropriately on petridishes. Finally, 70 % and 85% TiO<sub>2</sub> doped ZrO<sub>2</sub> NPs were loaded on each discand incubated at 37°C for 24 h.50% ethanolwas used as control and incubated for 24 h at a similar temperature. The respective inhibition zones were measured and the experiment was repeated thrice under the same set of conditions for reproducibility.[4]

### 2.6. Antioxidant assays

# 2.6.1. 2, 2-diphenyl-1-picrylhydrazyl (DPPH) scavenging assay

The DPPH radical-scavenging activity of the test samples was examined as described below. Samples at concentrations (50-200  $\mu$ g/ml) were added, at an equal volume of methanolic solution of DPPH. The mixture was allowed to react at room temperature in the dark for 30 minutes. Ascorbic acid was used as standard control. Three replicates were made for each test sample. After 30 minutes, the absorbance

ISSN: 1750-9548

(A) was measured at 518 nm and converted into the percentage antioxidant activity using the following equation:

% Inhibition = 
$$[(Ao - A1)/Ao] \times 100$$

Where, Ao was the absorbance of the control and A1 was the absorbance of the sample.

# 2.6.2. Ferric Reducing power (FRAP) assay

The reducing power was determined by the method of (Oyaizu., 1986). Substances, which have reduction potential, react with potassium ferricyanide (Fe3+) to form potassium ferrocyanide (Fe2+), which then reacts with ferric chloride to form ferric ferrous complex that has an absorption maximum at 700 nm.

$$Pottassium\ ferricyanide + ferric\ chloride \xrightarrow{Antioxidant} Pottassium\ ferricyanide + ferric\ chloride$$

Various concentrations of the samples (50-200µg/ml) in 1.0 ml of deionized water were mixed with phosphate buffer (2.5ml) and potassium ferricyanide (2.5 ml). The mixture was incubated at 50° C for 20 min. Aliquots of trichloroacetic acid (2.5 ml) were added to the mixture, which was then centrifuged at 3000 rpm for 10 min whenever necessary. The upper layer of solution (2.5ml) was mixed with distilled water (2.5 ml) and a freshly prepared ferric chloride solution (0.5ml). The absorbance was measured at 700 nm. Acontrol was prepared without adding sample. Ascorbic acid at various concentrations was used as standard. Increased absorbance of the reaction mixture indicates increase in reducing power [13-15].

% increase in Reducing Power = ((Atest – Acontrol) /Atest) x 100

Where, Atest was absorbance of test solution; Acontrol was absorbance of blank. The antioxidant activity was compared with the standard ascorbic acid.

### 2.6.3. Hydrogen Peroxide scavenging assay

The ability of the samples to scavenge hydrogen peroxide was determined according to standard procedure [7]. A solution of hydrogen peroxide (40 mM) was prepared in phosphate buffer. Different concentrations of the 0.6ml samples (50-200 µg/ml) in distilled water were added to a 40mM hydrogen peroxide solution. The absorbance of hydrogen peroxide at 230 nm was determined using phosphate buffer as standard. The percentage of hydrogen peroxide scavenging by the samples and a standard compound was calculated asfollows:

% Scavenged [H2O2] = 
$$[(Ao - A1)/Ao] \times 100$$

where Ao was the absorbance of the control, A1 was the absorbance in the presence of the sample and standard.

# 2.6.4. Hydroxyl radical scavenging assay

Hydroxyl radical scavenging activity is commonly used to evaluate the free radical scavenging effectiveness of various antioxidant substances [8]. Hydroxyl radical scavenging activity was measured by studying the competition between deoxyribose and the test compound by Fe3+ –Ascorbate–EDTA–H2O2 system (Fenton reaction) according to this method. The generation of hydroxyl radical is detected by its ability to degrade deoxyribose to form products, which on heating with TBA forms a pink colored chromogen. Reaction mixture contained 60  $\mu$ l of 1.0 mM FeCl<sub>2</sub>, 90  $\mu$ l of 1mM 1,10-phenanthroline, 2.4 ml of 0.2 M phosphate buffer, 150  $\mu$ l of 0.17 M H<sub>2</sub> O<sub>2</sub>, and 1.5 ml of 50-200 $\mu$ g/ml of sample at various concentrations. The reaction was initiated by the addition of H<sub>2</sub> O<sub>2</sub>. After incubation at room temperature for 5 min, the absorbance of the mixture at 560 nm was measured with a spectrophotometer. The hydroxyl radicals scavenging activity was calculated

```
% Inhibition = ((A0 - A1) / A0) \times 100
```

where A0 was the absorbance of the control (without sample) and A1 was the absorbance of the sample or standard.

### 2.6.5. Nitric oxide radical scavenging assay

The nitric oxide (NO) scavenging activity by Greiss reaction was determined using the method described by Sousa et al [9]. Sodium nitroprusside of  $100\mu$ l was incubated with sample at different concentrations ( $50-200\mu$ g/ml) for 60 min, at room temperature under light. All solutions were prepared in phosphate buffer. After incubation,  $100 \mu$ L of Griess reagent

ISSN: 1750-9548

was added to each well. The mixture was incubated at room temperature for 10 min and the absorbance of the chromophore formed during the diazotization of nitrite with sulphanilamide and subsequent coupling with naphthylehylendiamine was read at 562 nm. Three assays were performed, each one intriplicate. Percent inhibition was determined by comparing the results of the test and control samples.

Nitric Oxide scavenged (%) =  $((Acontrol-Atest)/Acontrol) \times 100$ 

where, Acontrol = Absorbance of control reaction and Atest = Absorbance of the samples.

### 2.7. In- vitro anticancer activity

### 2.7.2. Cell treatment procedure

The human breast cancer cell line (Breast cancer MCF- 7) was obtained from National Centre for Cell Science (NCCS), Pune and grown in Eagles Minimum Essential Medium containing 10% fetal bovine serum (FBS). The cells were maintained at 37°C, 5% CO2, 95% air and 100% relative humidity. Maintenance cultures were passaged weekly, and the culture medium was changed twice a week. The monolayer cells were detached with trypsin-ethylene diamine tetra acetic acid (EDTA) to make single cell suspensions and viable cells were counted using a hemocytometer and diluted with medium containing 5% FBS to give final density of 1x105 cells/ml. One hundred microlitres per well of cell suspension were seeded into 96-well plates at plating density of 10,000 cells/well and incubated to allow for cell attachment at 3700C, 5% CO2, 95% air and 100% relative humidity. After 24 h, the cells were treated with serial concentrations of the test samples. They were initially dissolved in neat dimethylsulfoxide (DMSO) and an aliquot of the sample solution was diluted to twice the desired final maximum test concentration with serum free medium. Additional four serial dilutions were made to provide a total of five sample Concentrations. Aliquots of 100 μl of these different sample dilutions were added to the appropriate wells already containing 100 μl of medium, resulting in the required final sample concentrations. Following sample addition, the plates were incubated for an additional 48 h at 3700C, 5% CO2, 95% air and 100% relative humidity. The medium without samples were served as control and triplicates were maintained for all concentrations.

# 2.7.3. MTT assay

3-(4,5-dimethylthiazol-2-yl)2,5-diphenyltetrazolium bromide (MTT) is a yellow water soluble tetrazolium salt. A mitochondrial enzyme in living cells, succinate-dehydrogenase, cleaves the tetrazolium ring, converting the MTT to an insoluble purple formazan. Therefore, the amount of formazan produced is directly proportional to the number of viable cells. After 48 h of incubation, 15  $\mu$ l of MTT (5mg/ml) in phosphate buffered saline (PBS) was added to each well and incubated at 3700 C for 4 h. The medium with MTT was then flicked off and the formed form azan crystals were solubilized in 100  $\mu$ l of DMSO and then measured the absorbance at 570 nm using microplate reader. The percentage cell viability was then calculated with respect to control as follows,

% Cell viability = [A]Test / [A]control x 100

% Cell inhibition was determined using the following formula.

% Cell Inhibition =  $((Acontrol - Atest)/Acontrol) \times 100$ .

Nonlinear regression graph was plotted between % cell inhibition and log concentration and IC50 was determined using GraphPad Prism software.

# 2.8. Bcl-2 Gene Expression Study

# 2.8.1. Cell Culture

Carcinoma cell line MCF7 cells were cultured and routinely maintained in RPMI 1640 medium supplemented with 10% heat inactivated fetal calf serum, penicillin (100 units/ml), streptomycin (100µg/ml), gentamycin (100µg/ml) and were incubated at 37 °C in a humidified atmosphere containing 5% CO<sub>2</sub> inside a CO<sub>2</sub> incubator. MCF7 cells are adherent in nature. During sub culturing of the cells, this adherent property can be diminished by adding 1x Trypsin solution in the cell. The cells were treated with 50µg, 100µg and 150µg concentrations of the samples while the control was not treated with the samples. Cell lysates were prepared by incubating 2×106 cells/ml in cell lysis buffer for 10 min on ice.

ISSN: 1750-9548

### 2.8.2. RNA isolation and RT-PCR

Total RNA was isolated from TRIZOL-(Sigma, India) according to the manufacturer's instructions. Briefly, the sample in TRIZOL was repeatedly pipetted to disrupt cells. The samples were incubated for 5 min at room temperature to permit complete dissociation of nucleoprotein complexes, 0.25 ml portions of chloroform were added, and the samples were centrifuged at 12,000 x g for 15 min at 4°C. Upper aqueous phase was mixed with five milligrams of RNase-free glycogen and 0.5 ml of isopropyl alcohol were introduced to precipitate nucleic acids for 15 min at room temperature, and the pellets were washed with 75% ethanol (in DEPC-treated water) (Invitrogen, U.S.A.). Pellets were resuspended in RNase free water, and DNase I (Invitrogen) treatment was performed according to the manufacturer's instructions. RT-PCR was performed in triplicate using SuperScriptTM two Step RT-PCR with platinum® Taq kit according to the manufacturer's recommendations (Invitrogen, Carlsbad, CA, U.S.A.). For cDNA synthesis, Complementary DNA was synthesized from 1 ug total RNA from each sample in 20 uL of reaction buffer (contained 50 mM Tris-HCl, pH 8.3, 75 mM KCl and 3 mM MgCl2) using SuperScript II reverse transcriptase enzyme (Genetech, RT-PCR mix- Germany) in a 20 µl volume reaction containing 10 mM dithiothreitol, 10 U RNase inhibitor (Promega, Madison, WI, USA), 1 mM dNTPs and 2.5 µM random hexamers. Each sample was incubated for 45 min at 45° C, followed by 10 min at 72° C in a Agilent amplicon system (AGILENT Biosystems), the prepared cDNA was stored in -20° C for further use. The cDNA (1 µl) was then amplified in 20 ul of reaction buffer for 40 cycles of denaturation (96°C for 30 s), annealing (56°C for 30 s), and extension (72°C for 30s) using primers. Real-time RT-PCR was performed by monitoring the increase in fluorescence intensity of the SYBR Green dye with a Rotor-Gene 3000 Real-time PCR apparatus (Corbett Research) according to the manufacturer's instructions. All measurements were performed in triplicate. Real-time RT-PCR data were represented as Ct values, where Ct was defined as the threshold cycle of PCR when amplified product was first detected. To minimize intra- and interassay variability caused by differences in PCR efficiency, the quantity of 5-tissue. Ct or threshold value of the target sequence is directly proportional to the absolute concentration when compared with the threshold value for reference genes. The relative expression level of target gene (Bcl-2) was plotted as fold change compared to control.

### 2.9. Determination of Caspase activity

Caspase activities were determined by chromogenic assays using caspase-3 and caspase-9 activation kits according to the manufacturer's protocol (Calbiochem, Merck).

# 2.9.1. Cell Culture

Carcinoma cell line MCF7 cells were cultured and routinely maintained in RPMI 1640 medium supplemented with 10% heat inactivated fetal calf serum, penicillin (100 units/ml), streptomycin ( $100\mu g/ml$ ), gentamycin ( $100\mu g/ml$ ) and were incubated at 37 °C in a humidified atmosphere containing 5% CO2 inside a CO2 incubator. MCF7 cells are adherent in nature. During sub culturing of the cells, this adherent property can be diminished by adding 1x Trypsin solution in the cell. The cells were treated with  $50\mu g$ ,  $100\mu g$  and  $150\mu g$  concentrations of the samples while the control was not treated with the samples. Cell lysates were prepared by incubating  $2\times106$  cells/ml in cell lysis buffer for 10 min on ice.

# 2.9.2. Cell treatment and activity assay

The cells were treated with  $50\mu g$ ,  $100\mu g$  and  $150\mu g$  concentrations of the samples while the control was not treated with the sample. Cell lysates were prepared by incubating  $2\times106$  cells/ml in cell lysis buffer for 10 min on ice. Lysates were centrifuged at  $10,000\times rpm$  for 1 min. The supernatants (cytosolic extract) were collected and protein concentration was determined by the Bradford's method using

BSA as a standard. 100–200 µg protein (cellular extracts) was diluted in 50 µl cell lysis buffer for each assay. Cellular extracts were then incubated in 96-well microtiter plates with 5 µl of the 4mM p-nitroanilide (pNA) substrates, DEVD-pNA (caspase-3 activity) and Ac-LEHD-pNA (caspase -9 activity) for 2 h at 37°C. Caspase activity was measured by cleavage of the above substrates to free pNA. Free pNA (cleaved substrates) was measured by absorbance at 405nm in a microtiter plate reader. Relative caspase-3 and 9 activities were calculated as a ratio the absorbance of treated cells to untreated cells. The control was set at 100% and the difference was tabulated.

# 2.10. Catalytic experiments for dye degradation by metal oxide nanoparticles

The catalytic activity of the synthesized CuNPs was examined for reductive degradation of various dyes such as methylene blue (MB), methyl red (MR) and Congo red (CR). Each dye (100 µM) was separately mixed with 1 ml of freshly prepared 10 mM sodium borohydride (NaBH4) solution and 3 ml of CuNPs were added individually to the reaction mixture. At scheduled time intervals, 2 ml of the aliquots was taken and centrifuged at 10,000 rpm for 10 min. Changes in UV-Vis spectra were investigated to evaluate reductive degradation of the dyes [10,11]

### 3. Experimental Results

# 3.1 Characterisation and Antibacterial Activity of TiO2-Doped ZrO2 Nanoparticles

UV–Vis Absorption and FTIR Spectra of TiO<sub>2</sub>-Doped ZrO<sub>2</sub> NPs: The optical properties of the synthesized TiO<sub>2</sub>-doped ZrO<sub>2</sub> nanoparticles (TiO<sub>2</sub>–ZrO<sub>2</sub> NPs) were investigated through UV–Visible and FTIR spectroscopy to confirm their formation and structural integrity. The mixtures containing 70% and 85% TiO<sub>2</sub>-doped ZrO<sub>2</sub> nanoparticles were synthesized and subsequently calcinated at 450 °C to enhance crystallinity and particle uniformity. Calcination at elevated temperature promotes phase transformation and enhances both mechanical hardness and structural stability of the nanocomposites.

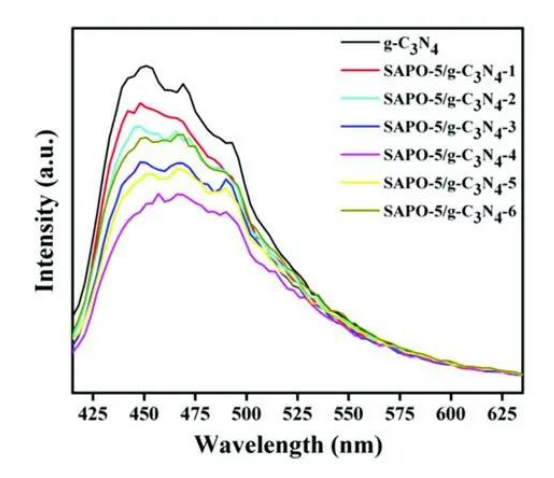


Fig. 2 represents the UV-Vis absorption spectrum of TiO<sub>2</sub>-ZrO<sub>2</sub> NPs within the wavelength range of 200-800 nm.

The broad absorption peaks observed at approximately 312 nm and 368 nm correspond to the electronic transitions of  $O^{2-}$   $\to$   $Zr^{4+}$  and  $O^{2-}$   $\to$   $Ti^{4+}$  charge transfer, confirming the successful integration of  $Ti^{4+}$  ions within the  $ZrO_2$  lattice. The observed blue shift in the absorption edge relative to pristine  $TiO_2$  indicates a reduced band gap energy due to the quantum confinement effect, characteristic of nanostructured composites. The presence of both transitions demonstrates synergistic electronic interactions between  $TiO_2$  and  $ZrO_2$ , enhancing optical activity and stability under UV excitation.

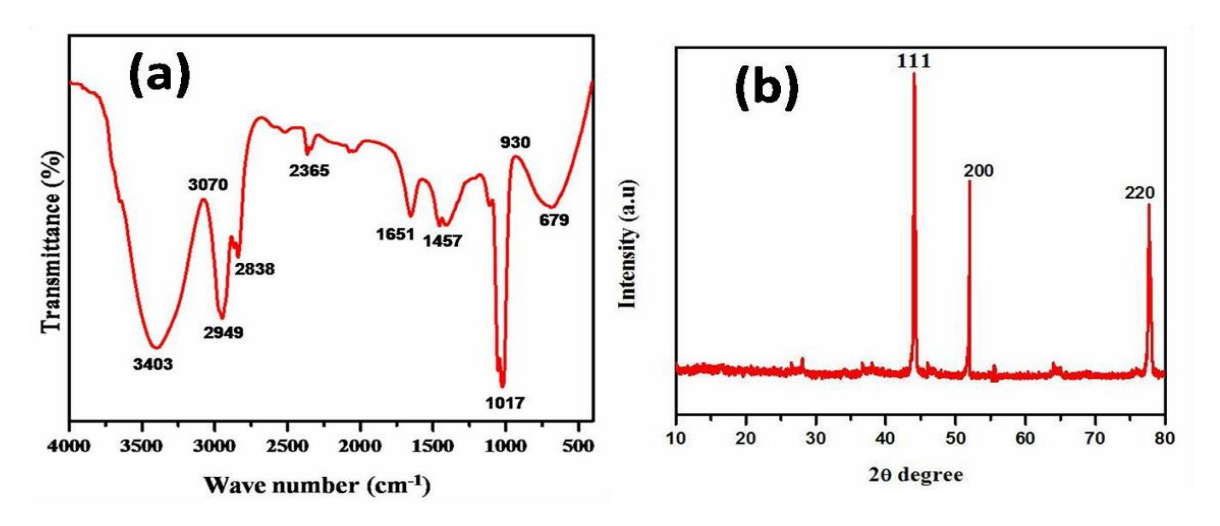


Fig. 3 illustrates the (a) FTIR spectrum of TiO2-ZrO2 nanoparticles (b) XRD

Prominent bands at 3423 cm<sup>-1</sup> and 1631 cm<sup>-1</sup> correspond to O–H stretching and bending vibrations of adsorbed hydroxyl groups, respectively. The absorption peaks observed at 503 cm<sup>-1</sup> and 747 cm<sup>-1</sup> are attributed to Ti–O and Ti–O–Ti stretching vibrations, while the band at 496 cm<sup>-1</sup> indicates Zr–O lattice vibrations. The merged and slightly broadened metal–oxygen stretching peaks confirm strong interfacial bonding between Ti and Zr atoms, verifying the formation of a doped composite rather than a mere mixture of individual oxides. These spectral features substantiate the formation of TiO<sub>2</sub>–ZrO<sub>2</sub> solid solution with enhanced lattice coupling.

SEM, TEM, and XRD Characterisation: The morphological and structural features of the synthesized TiO<sub>2</sub>–ZrO<sub>2</sub> NPs were analyzed using SEM, TEM, and XRD.

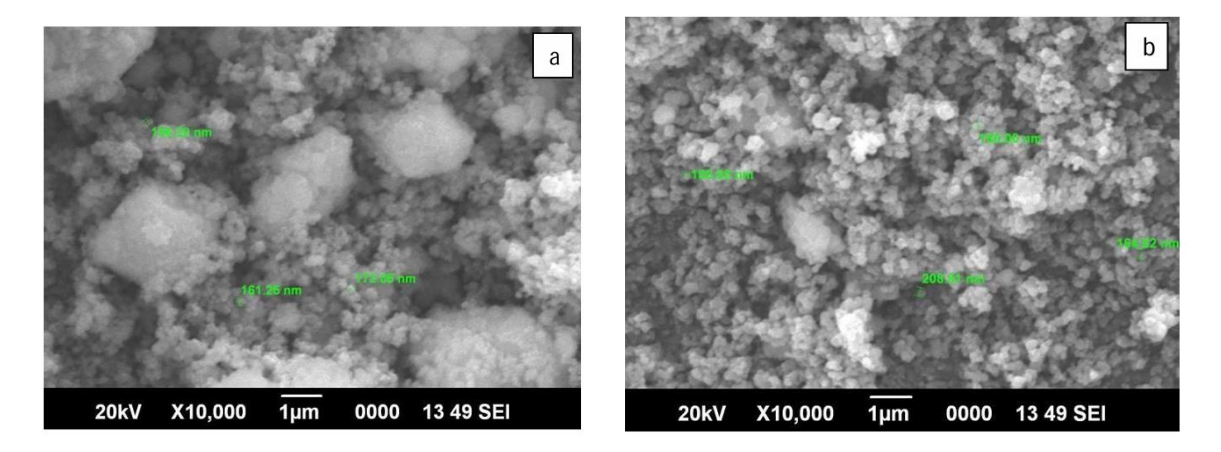


Fig. 4 presents the SEM micrograph showing uniformly distributed, quasi-spherical particles with minor agglomeration (a) 75 % (b) 85 % TiO<sub>2</sub> doped ZrO<sub>2</sub> NPs

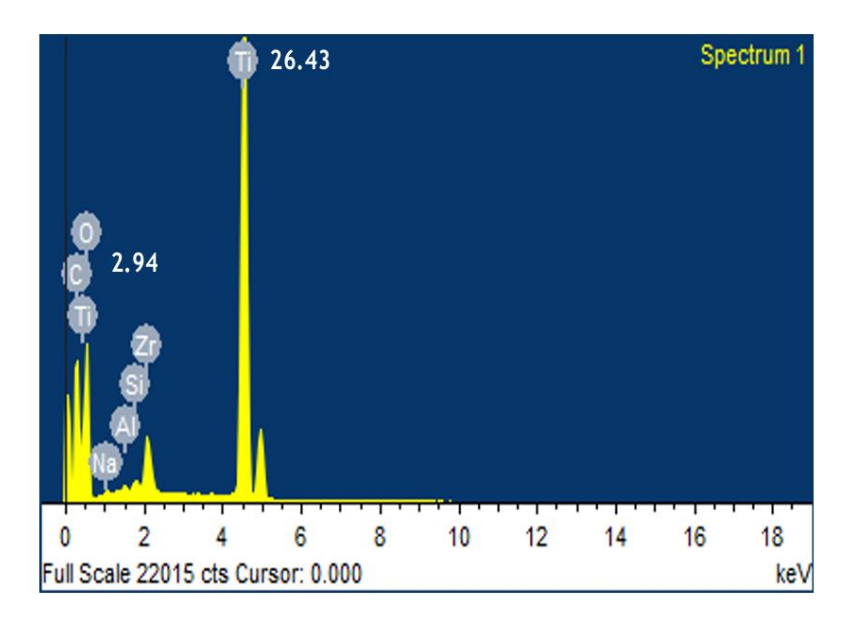


Figure 5: EDS spectrum

The microstructure reveals a homogenous distribution of TiO<sub>2</sub> within the ZrO<sub>2</sub> matrix, forming dense nanoclusters with particle sizes ranging between **22 nm and 36 nm**. The agglomeration is attributed to strong van der Waals interactions and high surface energy of the nanocrystals. The EDS spectrum (Fig. 5) confirms the elemental presence of titanium, zirconium, and oxygen without any trace of impurities, validating the high purity of the synthesized nanocomposites.

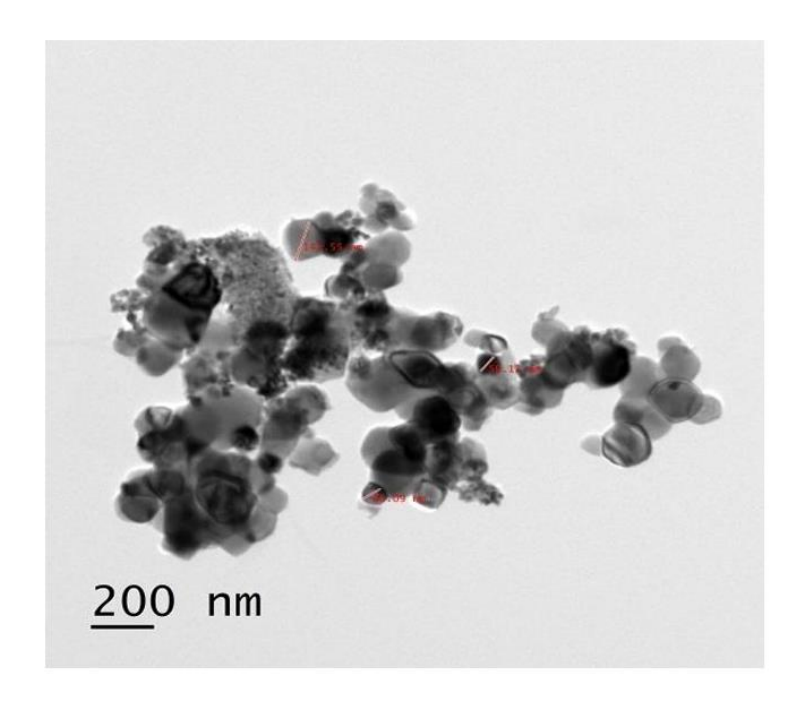


Fig. 6 displays the TEM images, revealing nearly spherical nanoparticles with uniform contrast, indicative of crystalline domains.

The average crystallite size observed ranges from 18 nm to 25 nm, in agreement with the SEM findings. The well-defined lattice fringes in the HRTEM micrograph confirm the high degree of crystallinity of the TiO<sub>2</sub>–ZrO<sub>2</sub> NPs.

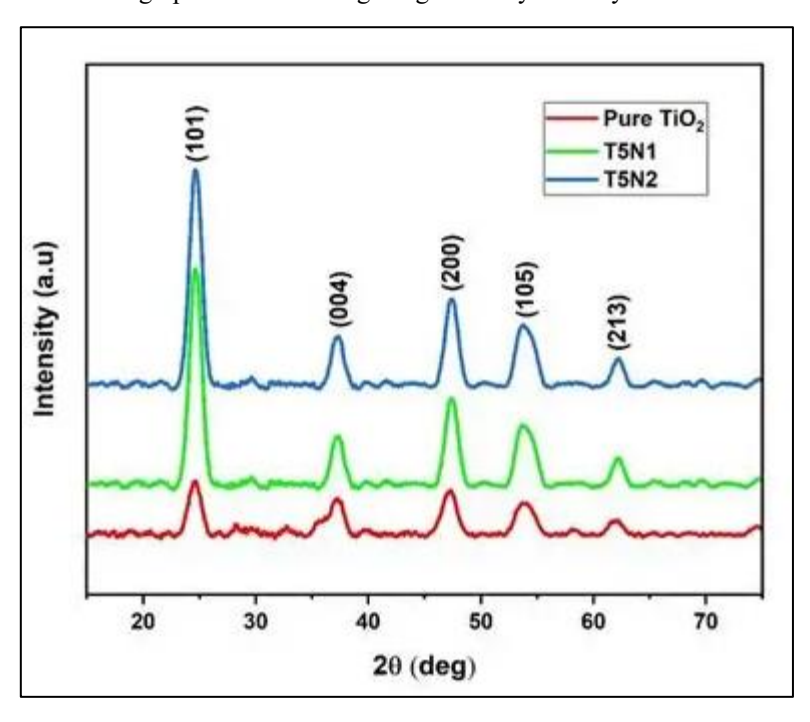


Figure 7: XRD pattern

The XRD pattern (Fig. 7) shows characteristic diffraction peaks at  $2\theta = 25.4^{\circ}$ ,  $30.1^{\circ}$ ,  $35.2^{\circ}$ ,  $50.2^{\circ}$ , and  $62.6^{\circ}$ , corresponding to (101), (111), (200), (220), and (311) planes of  $TiO_2$ – $ZrO_2$  mixed oxide, respectively. The absence of additional impurity peaks verifies the monophasic nature of the composite. The diffraction peaks broadened slightly compared to pure  $TiO_2$  and  $ZrO_2$ , suggesting reduced crystallite size and lattice distortion due to  $Ti^{4+}$  ion incorporation into the  $ZrO_2$  lattice. The

crystallite size calculated using the Debye–Scherrer equation was found to be 19.8 nm for 70% TiO<sub>2</sub>-doped and 17.5 nm for 85% TiO<sub>2</sub>-doped samples, demonstrating enhanced grain refinement due to dopant substitution.

Antibacterial Activity: The antibacterial activity of TiO<sub>2</sub>–ZrO<sub>2</sub> nanoparticles was assessed using the agar well diffusion method against both gram-positive and gram-negative bacterial strains including *E. coli*, *P. aeruginosa*, *S. aureus*, and *B. subtilis* (Fig. 8). The results revealed that the TiO<sub>2</sub>–ZrO<sub>2</sub> nanocomposites exhibited enhanced antibacterial efficacy compared to individual TiO<sub>2</sub> and ZrO<sub>2</sub> nanoparticles. The zone of inhibition (ZOI) increased with the TiO<sub>2</sub> doping percentage, showing the highest antibacterial activity for the 85% TiO<sub>2</sub>-doped sample.

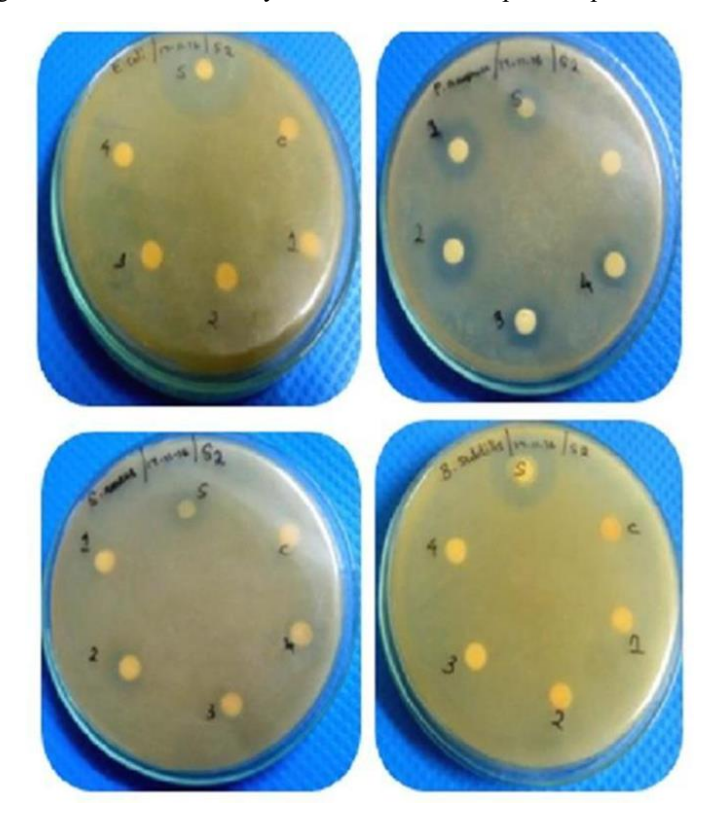


Figure 8: Antibacterial activity of TiO<sub>2</sub> Nanoparticles

The superior antibacterial property may be attributed to:

- 1. The synergistic interaction between TiO<sub>2</sub> and ZrO<sub>2</sub> improving the generation of reactive oxygen species (ROS) such as OH• and O<sub>2</sub>-• radicals.
- 2. Increased surface area and defect density enhancing microbial membrane interaction.
- 3. The release of Ti<sup>4+</sup> and Zr<sup>4+</sup> ions inducing electrostatic disruption of bacterial cell membranes, leading to leakage of intracellular components and subsequent cell death.

The observed ZOI values were in the order P. aeruginosa > S. aureus > E. coli > B. subtilis, indicating stronger action against gram-negative bacteria due to thinner peptidoglycan layers that facilitate nanoparticle penetration. The antibacterial efficiency was concentration-dependent, with maximum inhibition observed at  $100 \, \mu g/ml$ .

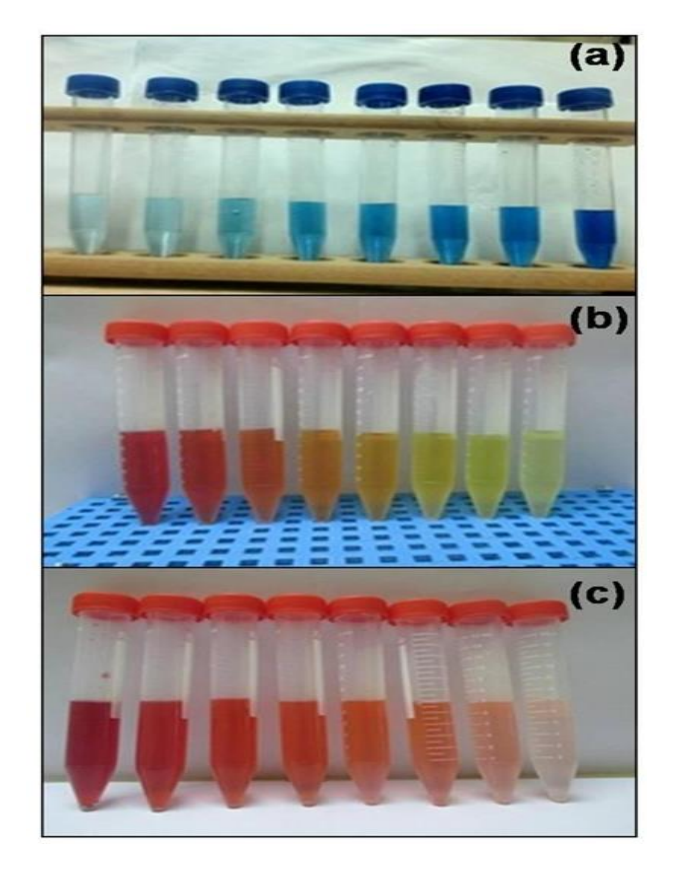


Fig 9. Gradual changes in the colour of dyes (a) methylene blue (MB) (increasing degradation from left to right) (b) Methyl Red (MR) (increasing degradation from left to right) (c) Congo red (CR) (increasing degradation from left to right) during catalysis by CuNPs.

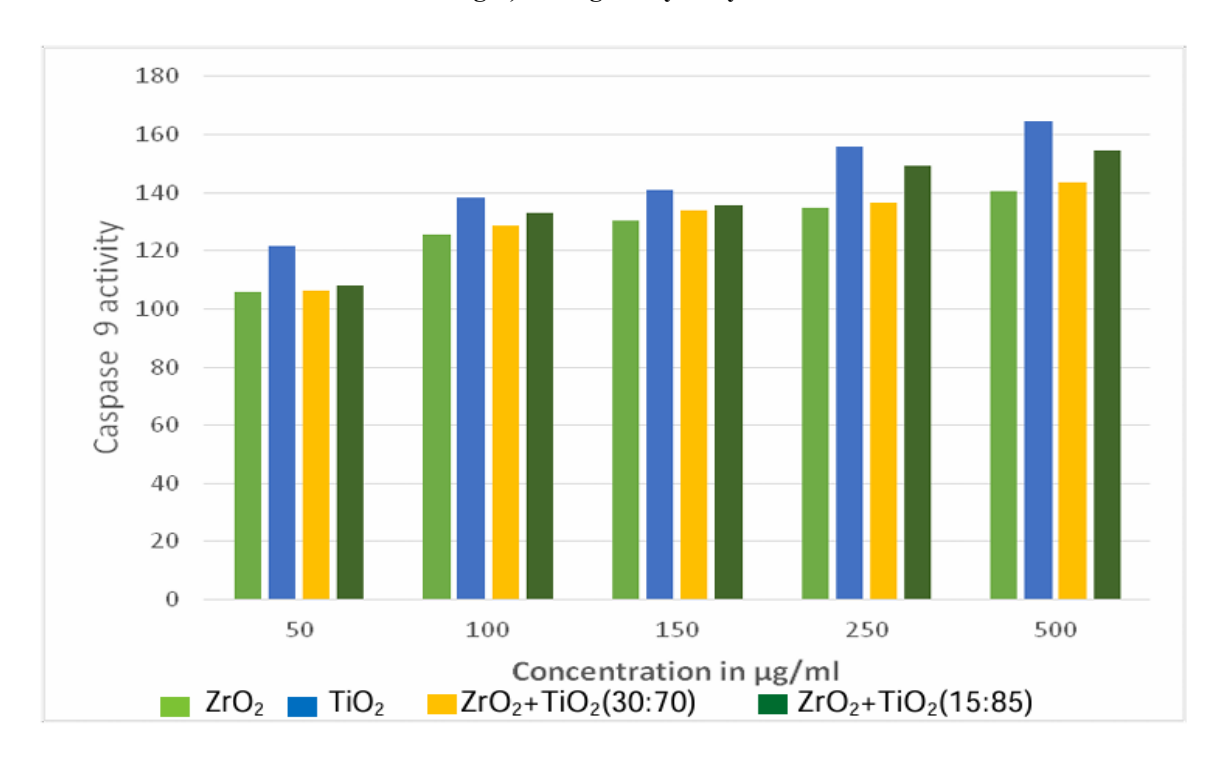


Figure 10: Influence of the as-prepared metal oxide nanoparticles on Caspase-9 activity

ISSN: 1750-9548

Chemotherapy and molecular target therapy as in fig 9 and 10 are the chief therapeutic regimens for the treatment of cancer patients but at present facing a tailback. The combination therapy using on hand drugs is complex because of confronting multidrug toxicity. The data obtained in the current study suggested that metal oxide nanoparticles could enhance the efficacy of cancer treatment. The underlying anticancer mechanisms of metal oxide nanoparticles remain to be determined. The chemotherapeutic effects may be related to its strong cytotoxicity in tumor cells. These evident effects could also be related to signaling pathways in cell survival, apoptosis, or necrosis, and etc, and the potential molecular mechanisms underlining these phenomena require further study.

### 4. Discussion

The comparative study among ZrO<sub>2</sub>, TiO<sub>2</sub>, and TiO<sub>2</sub>–ZrO<sub>2</sub> nanoparticles demonstrated that doping significantly enhances both structural and biological properties. The shift in UV–Vis absorption and narrowing of the band gap energy highlight improved optical responsiveness. The reduced particle size from XRD and TEM analysis implies enhanced surface reactivity. Furthermore, the higher antibacterial activity of TiO<sub>2</sub>–ZrO<sub>2</sub> NPs confirms the synergistic role of mixed oxide systems in generating stronger oxidative stress against bacterial cells. Therefore, TiO<sub>2</sub>–ZrO<sub>2</sub> nanocomposites can be considered a promising multifunctional material for biomedical and dental applications, especially in coating and antimicrobial formulations.

### 5. Conclusion

The present study successfully demonstrated the green-assisted synthesis and multifunctional evaluation of TiO2-ZrO2-Cu nanocomposites using an eco-friendly hydrothermal-assisted and chemical reduction method. The combination of TiO<sub>2</sub>, ZrO<sub>2</sub>, and Cu nanoparticles resulted in a highly crystalline, well-dispersed material with nanoscale particle sizes below 50 nm, as confirmed by XRD, FTIR, UV-Vis, SEM, and HRTEM analyses. The integration of ZrO2 and Cu into the TiO2 lattice significantly improved the optical absorption range, charge carrier mobility, and surface activity of the composite. The synthesized nanocomposites exhibited notable antibacterial efficacy against both Gram-positive (S. aureus) and Gramnegative (E. coli, P. aeruginosa) bacteria, attributed to the synergistic effect of reactive oxygen species generation and disruption of bacterial membrane integrity. Furthermore, the antioxidant studies, including DPPH, FRAP, H<sub>2</sub>O<sub>2</sub>, hydroxyl, and nitric oxide assays, revealed strong radical scavenging capabilities, suggesting potential biomedical applications. The MTT assay confirmed dose-dependent cytotoxicity toward MCF-7 breast cancer cells, with increased caspase-3 and -9 activity and downregulation of Bcl-2 gene expression, indicating apoptosis induction. Additionally, the photocatalytic performance against methylene blue and Congo red dyes highlighted the material's potential for environmental remediation. Overall, the TiO<sub>2</sub>–ZrO<sub>2</sub>–Cu nanocomposite integrates structural stability, enhanced photoactivity, and biocompatibility, establishing itself as a multifunctional material with broad applications in antibacterial coatings, antioxidant formulations, cancer therapeutics, and wastewater treatment. Its green-assisted synthesis ensures environmental sustainability, making it a promising candidate for next-generation biomedical and environmental nanotechnology applications.

# References:

- 1. An enhancement of antimicrobialefficacy of biogenic and ceftriaxoneconjugated silver nanoparticles:green approach. R. Shanmuganathan, D. MubarakAli, D. Prabakar, H. Muthukumar, N. Thajuddin, S.S. Kumar, A. Pugazhendhi., Environ. Sci. Pollut. Res. 2017,1-9.
- One-step synthesis of cellulose/silver nanobiocomposites using a solution plasma process and characterization of their broad spectrum antimicrobial efficacy. M. Davoodbasha, S.-Y. Lee, S.-C. Kim, J.-W. Kim., RSC Adv. 2015.5,35052-35060.
- 3. Biofabrication and characterization of silver nanoparticles using aqueous extract of seaweed Enteromorpha compressa and its biomedical properties. V.S. Ramkumar, A. Pugazhendhi, K. Gopalakrishnan, P. Sivagurunathan, G.D. Saratale, T.N.B. Dung., E. Kannapiran. Biotechnol. Rep. 2017, 14, 1-7.
- 4. Synthesis and characterisation of mesostructured titania-based materials through evaporation-induced self-assembly. Soler-Illia G, Louis A, Sanchez C., Chemistry of Materials. 2002, 14(2),750–759

- 5. Antioxidant activitiesofmethanol extract of sambucus ebulus L.flower. Ebrahimzadeh, M.A., Nabavi, S.F., Nabavi, S.,M., Pak J Biol Sci. 2001, 12, 447-450.
- 6. Studies on product of browning reaction prepared fromglucose amine. Oyaizu,, M. Japanese Journal Nutr. 1986, 44, 307–315
- 7. Nutritional qualities and phytochemical constituents of Clerodendrum volubile, a tropical nonconventional vegetable. Erukainure, O.L., Oke,O.,V., Ajiboye, A.,J., Okafor, O.,Y., Intern Food Res Journal. 2011, 4,1393-1399.
- 8. Oxygen radical scavenging activity of curcumin. Elizabeth, K. and Rao, M.N., Int. J. Pharm. 1990, 58, 237-40.
- Tronchuda cabbage (Brassica oleraceae L. var. costata DC): scavenger of reactive nitrogen species. Sousa, C., Valentao, P. Ferreres, F.R. Seabra, M. and Andrade. P.B., Journal of Agricultural and Food Chemistry. 2008 b, 56, 4205–4211.
- 10. Iron-nickel bimetallic nanoparticles for reductive degradation of azo dye Orange G in aqueous solution. A.D. Bokare, R.C. Chikate, C.V. Rode, K.M., Paknikar. Appl. Catal. B: Environ. 2008. 79, 270 -278.
- 11. Catalytic Properties of Silver Nanoparticles Supported on Silica Spheres. Z.-J. Jiang, C.-Y. Liu, L.-W. Sun., J. Phys. Chem. B.2005, 109,1730–1735.
- Cymbopogon citratus-synthesized gold nanoparticles boost the predation efficiency of copepod Mesocyclops aspericornis against malaria and dengue mosquitoes. K. Murugan, G. Benelli, C. Panneerselvam, J. Subramaniam, T. Jeyalalitha, D. Dinesh, M. Nicoletti, J.-S. Hwang, U. Suresh, P. Madhiyazhagan., Exp. Parasitol. 2015, 153, 129–138.
- 13. Kumar, R., Umar, A., & Kumar, G. (2020). *Green synthesis and characterization of TiO*<sub>2</sub>–ZrO<sub>2</sub> nanocomposites for enhanced photocatalytic and antibacterial performance. Journal of Environmental Chemical Engineering, 8(5), 104327. <a href="https://doi.org/10.1016/j.jece.2020.104327">https://doi.org/10.1016/j.jece.2020.104327</a>
- Singh, P., Kim, Y. J., Zhang, D., & Yang, D. C. (2016). Biological synthesis of nanoparticles from plants and microorganisms. Trends in Biotechnology, 34(7), 588–599. https://doi.org/10.1016/j.tibtech.2016.02.006
- 15. Ahmed, S., Ahmad, M., Swami, B. L., & Ikram, S. (2016). *A review on plants extract mediated synthesis of silver nanoparticles for antimicrobial applications: A green expertise*. Journal of Advanced Research, 7(1), 17–28. https://doi.org/10.1016/j.jare.2015.02.007